npj | Materials Degradation

www.nature.com/npjmatdeg

ARTICLE OPEN

# Multi-scale investigation of uranium attenuation by arsenic at an abandoned uranium mine, South Terras

Claire L. Corkhill[1], Daniel E. Crean[2], Daniel J. Bailey[1], Carmen Makepeace[1], Martin C. Stennett[1], Ryan Tappero[3], Daniel Grolimund[4] and Neil C. Hyatt[1]

Detailed mineralogical analysis of soils from the UK's historical uranium mine, South Terras, was performed to elucidate the mechanisms of uranium degradation and migration in the 86 years since abandonment. Soils were sampled from the surface (0–2 cm) and near-surface (25 cm) in two distinct areas of ore processing activities. Bulk soil analysis revealed the presence of high concentrations of uranium (<1690 p.p.m.), arsenic (1830 p.p.m.) and beryllium (~250 p.p.m.), suggesting pedogenic weathering of the country rock and ore extraction processes to be the mechanisms of uranium ore degradation. Micro-focus XRF analysis indicated the association of uranium with arsenic, phosphate and copper; μ-XRD data confirmed the presence of the uranyl-arsenate minerals metazeunerite ($Cu(UO_2)_2(AsO_4)_2{\cdot}8H_2O$) and metatorbernite ($Cu(UO_2)_2(PO_4)_2{\cdot}8H_2O$) to be ubiquitous. Our data are consistent with the solid solution of these two uranyl-mica minerals, not previously observed at uranium-contaminated sites. Crystallites of uranyl-mica minerals were observed to coat particles of jarosite and muscovite, suggesting that the mobility of uranium from degraded ores is attenuated by co-precipitation with arsenic and phosphate, which was not previously considered at this site.

*npj Materials Degradation* (2017)1:19 ; doi:10.1038/s41529-017-0019-9

## INTRODUCTION

The UK's most important uranium-producing mine, South Terras, is located in the St. Austell District of Cornwall (SW England, Supplementary Fig. 1), which operated between 1873 and 1930. The primary ore, pitchblende (primarily $UO_2$ and $U_3O_8$), is associated with late stage metamorphism related to the St. Austell granitic intrusion, formed 225 Ma.[1] Secondary uranium-ores of torbernite ($Cu(UO_2)_2(PO_4)_2{\cdot}12H_2O$) and autunite ($Ca(UO_2)_2(PO_4)_2{\cdot}12H_2O$) formed 60 Ma.[2,3] In the 57 year period of operation before closure, South Terras produced 736 tonnes of uranium.[1] The discovery of radium, in 1911, focused mining operations on the uranium spoil heaps at the site, which were investigated by Marie Curie.[1] The tailings were reworked to extract radium through $BaSO_4$ recovery methods.[1]

South Terras has been considered to be a "natural laboratory" for the environmental degradation and behaviour of naturally occurring radionuclides.[4–6] Previous investigations have attempted to elucidate the degradation process of uranium ores and the subsequent transport of uranium from the spoil heaps into the River Fal (Supplementary Fig. 1). Currently, two key hypotheses remain open: i) small uranium-rich particles are transported from the sediments to the stream[6] and/or; ii) uranyl-phosphate or uranyl-carbonate species are transported by groundwater.[4,7] To accurately predict the U(VI) transport processes with reactive transport models, detailed understanding of uranium ore degradation mechanisms and uranium speciation, from the macro-scale to the micro-scale, is necessary. We present the results of a detailed multi-modal micro-focus X-ray fluorescence spectroscopy and diffraction characterisation of South Terras soils, complemented with macro-scale analyses, and reveal the presence of important phases not previously considered in uranium speciation models of the site, which may influence the long-term release of uranium from the soils. This study contributes to the management of legacy uranium contamination at sites with a complex industrial history.

## RESULTS

### Bulk soil properties

XRD analysis revealed the ubiquitous presence of muscovite ($KAl_2(AlSi_3O_{10})(OH_2)$), quartz ($SiO_2$) and jarosite ($KFe_3(OH)_6(SO_4)_2$) (Supplementary Fig. 2), in agreement with previous analysis of soils from South Terras.[5,6] Additional goethite (FeO(OH)) and the zeolite, montesommaite ($(K,Na)_9Al_9Si_{23}O_{64}{\cdot}10H_2O$), were identified at the Ochre Works (OW) location, reflecting the different ore degradation mechanisms at this sample location.

Uranium-containing, sub-micron phases with a platy morphology were observed to coat the surfaces of lower z-contrast (i.e., not uranium-containing) particles. Figure 1 shows an example of this morphology in particles from 25 cm depth (Dressing Floor (DF) location). Elemental mapping analysis confirmed the presence of uranium, which was found to occur in association with arsenic, copper and phosphorus (Fig. 1). The underlying particle contained silicon, aluminium, sulphur and iron, which is in agreement with the XRD identification of muscovite and jarosite.

[1]Department of Materials Science and Engineering, NucleUS Immobilisation Science Laboratory, The University of Sheffield, Sheffield, UK; [2]Atomic Weapons Establishment plc, Aldermaston, Berkshire RG7 4PR, UK; [3]Photon Sciences Directorate, Brookhaven National Laboratory, Upton, NY, USA and [4]Swiss Light Source, Paul Scherrer Institute, Villigen 5232, Switzerland
Correspondence: Claire L. Corkhill (c.corkhill@sheffield.ac.uk) or Neil C. Hyatt (n.c.hyatt@sheffield.ac.uk)

Received: 6 June 2017 Revised: 24 September 2017 Accepted: 29 September 2017
Published online: 14 December 2017

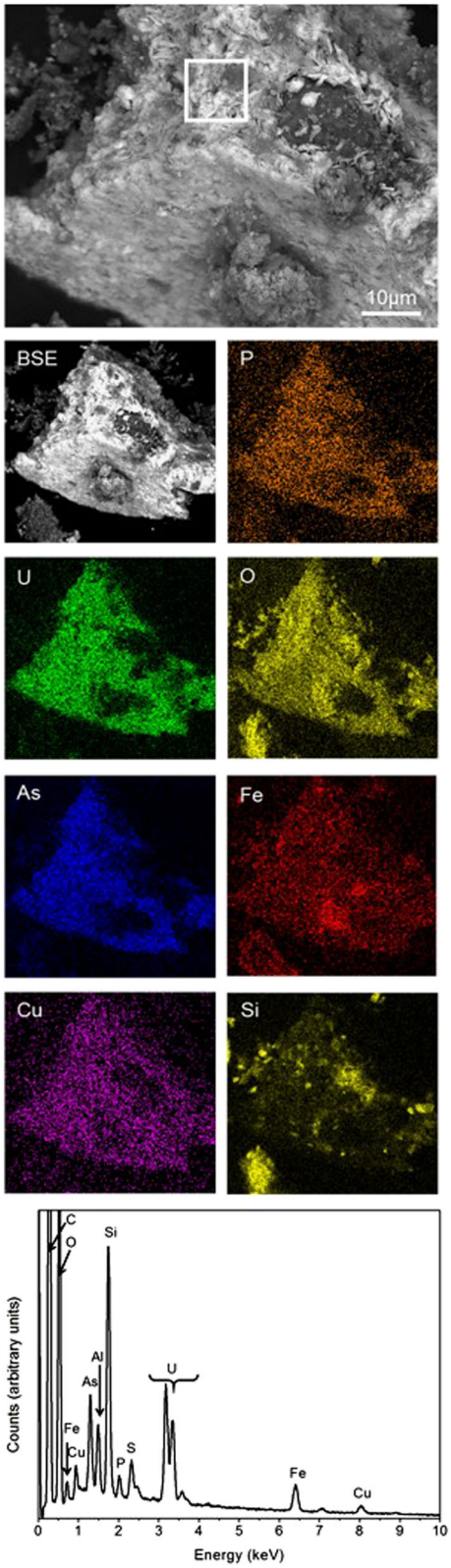


**Fig. 1** SEM and EDX analysis of a uranium-bearing particle in soil from the Dressing Floor location (25 cm), showing the uranium morphology and distribution of associated elements. EDX spectrum summed from map taken in the ROI indicated by the white square box

**Table 1.** Concentration of selected elements in South Terras soil locations, derived from total acid digest (residual fraction, Supplementary Table 2) and ICP-AES analysis

| | Elemental concentration (p.p.m.) | | |
|---|---|---|---|
| | Ochre Works 0–2 cm | Dressing Floor 25 cm | Dressing Floor 0–2 cm |
| Be | $(2.43 \pm 0.07) \times 10^2$ | $(2.49 \pm 0.07) \times 10^2$ | $(2.78 \pm 0.08) \times 10^2$ |
| P | $(1.22 \pm 0.73) \times 10^3$ | $(7.18 \pm 0.63) \times 10^2$ | $(1.35 \pm 0.02) \times 10^3$ |
| V | $(1.81 \pm 0.05) \times 10^2$ | $(9.20 \pm 0.30) \times 10^1$ | $(6.70 \pm 0.02) \times 10^1$ |
| Cu | $(3.15 \pm 0.12) \times 10^2$ | $(5.00 \pm 0.02) \times 10^2$ | $(5.18 \pm 0.07) \times 10^2$ |
| As | $(1.83 \pm 0.03) \times 10^3$ | $(3.28 \pm 0.06) \times 10^3$ | $(2.00 \pm 0.01) \times 10^3$ |
| Pb | $(1.22 \pm 0.05) \times 10^3$ | $(1.17 \pm 0.02) \times 10^3$ | $(2.87 \pm 0.14) \times 10^3$ |
| U | $(1.11 \pm 0.09) \times 10^2$ | $(1.69 \pm 0.37) \times 10^3$ | $(3.66 \pm 0.07) \times 10^2$ |

*Note*: Error estimates are ± 1 standard deviation of replicate (10) analysis. See Supplementary Table 1, for all elemental analysis

### Total acid digest analysis

Uranium concentrations, shown in Table 1, ranged from 111 ± 9 p.p.m. to 1690 ± 370 p.p.m. The uranium concentration in soils taken at 25 cm (DF location) was significantly higher than the two surface (0–2 cm) soils. Significant concentrations of arsenic were observed, ranging from 1830 ± 30 p.p.m. to 3280 ± 60 p.p.m., consistent with the mining activities at the site and also with pedogenesis of the country rock, which has been reported to contain the arsenate minerals scorodite ($FeAsO_4.2H_2O$) and pharmocosiderite [$(AsO_4)_3(OH)_3.6H_2O$].[3] Average stream water concentrations of arsenic in the vicinity of South Terras were recently determined as 99 p.p.m. by the TELLUS airborne geophysical survey,[8] which is significantly above the World Health Organisation drinking water limit of 0.1 p.p.m.[9] To our knowledge, despite detailed investigation of uranium at the site, the migration of arsenic to the River Fal has not previously been investigated.

Notably high beryllium concentrations were observed, at ~250 p.p.m., across the site (Table 1). The average crustal abundance of beryllium is 3 p.p.m., but in areas of pegmatitic igneous activity, soil concentrations can be elevated. Previously, beryllium has been identified in the St. Austell area, occurring in minerals such as danalite [$(Fe_4(Be_3Si_3O_{12})S$], phenacite ($Be_2SiO_4$) and bertrandite ($Be_4Si_2O_7(OH)_2$).[2] Although beryllium minerals were not identified in the present study, to our knowledge, elevated soil concentrations of beryllium at South Terras have not previously been reported.

### Sequential extraction analysis

The fraction of uranium determined in each extraction step, expressed as a percent of the total digest concentration (Table 1), is shown in Fig. 2. The greatest proportion of uranium was located in the residual and recalcitrant fractions, followed by the oxidisible fraction. The lowest proportion was observed in the reducible and exchangeable fractions. Elements that showed similar behaviour to uranium were arsenic, phosphorus and copper (Supplementary Fig. 3), suggesting that uranium is closely associated with these elements, in agreement with EDX analysis (Fig. 1).

### Micro-focus analysis of major uranium particles

To obtain a positive identification of the form of uranium present in South Terras soils, a combination of μ-XRF and μ-XRD analyses were performed. Micro-XRF was used to identify U-enriched particles and phase identification was subsequently performed by μ-XRD. Large uranium-bearing particles in all South Terras soils were associated with copper and arsenic, as shown by μ-XRF maps (Fig. 3a). Micro-XRD analysis of particles from 25 cm (DF location,

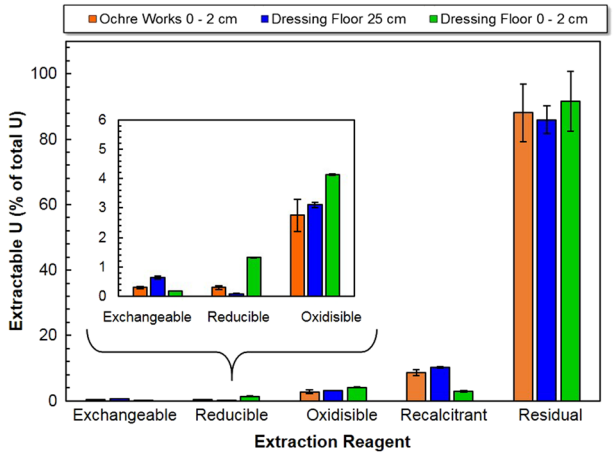


**Fig. 2** Fractionation of uranium between defined classifications for three soils at the South Terras site. Total elemental concentrations are given in Table 1. Error bars are one standard deviation of multiple (ten) replicates

Fig. 3b) is consistent with the structure of the uranyl mica family of minerals (space group P4/nz), which have a characteristic layered structure with alternating sheets of $[(UO_2)(XO_4)]^{-1}$, where X=P, As and hydrated $Cu^{2+}$ cations.[10] A number of compounds with the A $(UO_2)_2(XO_4)_2{\cdot}nH_2O$ structure exist, where A=Ca, Ba, Mg, $Cu^{2+}$, $Ni^{2+}$, $Pb^{2+}$ $Fe^{2+}$ including: metaautunite $(Ca(UO_2)_2(PO_4)_2{\cdot}8H_2O)$, a partially-dehydrated counterpart of the secondary South Terras uranium-ores, autunite; metatorbernite $(Cu(UO_2)_2(PO_4)_2{\cdot}8H_2O)$, and the arsenic end-member of the same family, metazeunerite $(Cu(UO_2)_2(AsO_4)_2{\cdot}8H_2O)$.

Rietveld analysis of the micro-XRD pattern in Fig. 3b gives lattice parameters of $a = 6.992(1)$ Å, $c = 17.318(4)$ Å and a lattice volume of 846.77(1) Å$^3$. These lattice parameters, combined with the significant concentration of As measured by μ-XRF, are suggestive of the presence of the copper and arsenic-bearing uranyl-mica, metazeunerite. However, EDX maps also suggest the presence of P (Fig. 1), which was not measured in the μ-XRF analysis due to the imposed energy cut-off; the refined lattice parameters and volume fall between those of metazeunerite and the phosphate end-member of the same family, metatorbernite ($a = 7.1094(1)$, $c = 17.146(1)$ and $v = 866.620(1)$ Å$^{\alpha}$ for metazeunerite, and $a = 6.9756(5)$, $c = 17.349(2)$ and $v = 844.184(3)$ Å$^3$ for metatorbernite).[11] Owing to the similar thermochemical radii of P and As (2.38 Å and 2.48 Å for phosphate and arsenate, respectively),[12] it is feasible that a solid solution of divalent interlayer anions exists between metazeunerite and metatorbernite.[13] The refined lattice parameters are closer in dimension to metazeunerite, therefore arsenic is expected to dominate over phosphorus in this solid solution of $Cu(UO_2)_2(AsO_4)_{2-x}(PO_4)_x{\cdot}8H_2O$. Assuming the solid solution to follow Vegards Law, our unit cell volume suggests ~18% solid solution of metatorbenite in metazeunerite. Metatorbernite has previously been reported to sequester uranium at other uranium-contaminated sites such as Hanford (USA)[14–17] and has also been reported to occur at South Terras[3]. Although the occurrence of metazeunerite at South Terras has been previously inferred,[18] to our knowledge, this study provides conclusive and verifiable evidence for this phase at the site, and indeed for any studied uranium-contaminated vadose sediments.[14–17]

In the μ-XANES analysis of the copper, uranium, arsenic particle shown in Fig. 3a, the reduced intensity of the white line, and the presence of a shoulder feature (labelled 'A', Fig. 3c) confirms that uranium is present as the uranyl ($UO_2^{2+}$) species, consistent with the presence of (a solid solution of) metazeunerite and metatorbernite. This feature is absent in compounds that do not contain the uranyl moiety. With reference to the measured uranium standards, which display a linear relationship between the uranium $L_{III}$-edge position and the oxidation state in the range U(IV) to U(VI) (Supplementary Fig. 4), the sample particle composed of metazeunerite and metatorbernite demonstrates a mean uranium oxidation state of 5.9 ± 0.4 (Table 2).

### Micro-focus analysis of minor uranium particles

Particles with uranium fluorescence counts one order of magnitude lower than observed in Fig. 3a were investigated. Co-location of uranium with rubidium, known to be present in high concentrations in the Cornubian granites, and often substituted for potassium in minerals such as muscovite,[19] necessitated a two-step analysis due to the closely overlapping fluorescence lines of U $L\alpha_1$ (13.614 keV) and Rb $K\alpha_1$ (13.396 keV), as illustrated in Fig. 4a. The difference in X-ray absorption at an incident energy above the U $L_{III}$ edge ($E_0 = 17.200$ keV, Fig. 4b) to that below the U $L_{III}$ edge ($E_0 = 16.900$ keV) served to distinguish concentrations of uranium from rubidium (Fig. 4c). Areas with an intensity <0 in Fig. 4c are related to rubidium, due to a reduction in the rubidium absorption cross section as the incident photon energy is increased, while those with an intensity >0 are related to uranium, due to the excitation of the $L_{III}$ edge exclusively at the higher energy. μ-XRD analysis of the point identified in Fig. 4c, belonging to a particle from 0–2 cm DF location, revealed the presence of quartz, plumbojarosite $(PbFe^{3+}{}_6(SO_4)_2(OH)_{12})$, muscovite $(KAl_2(Si_3Al)O_{10}(OH)_2)$ and kaolinite $(Al_2Si_2O_5(OH)_4)$. No reflections for uranium-bearing minerals could be fit to the data. In their study of uranium at the Hanford site, Catalano et al.[14] similarly found non-crystalline uranium bound to phyllosilicates. The mean uranium oxidation state in particles from this location ranged from 5.0 ± 0.4 to 6.0 ± 0.4 (Table 2, Supplementary Fig. 4); the partially reduced state may arise from reduction of uranium to $U_3O_8$ by Fe(II), e.g., in chlorite phyllosilicates.

The phases metatorbernite $(Cu(UO_2)_2(PO_4)_2{\cdot}8H_2O)$, jarosite $(KFe_3(OH)_6(SO_4)_2)$ and akaganeite (β-FeOOH) were observed in soils from 25 cm DF location (Supplementary Fig. 5a–c). The presence of metatorbernite, in this case isolated from metazeunerite, confirms the prevalence of uranyl-mica minerals in South Terras soils. The presence of iron-bearing jarosite and akaganeite are in agreement with EDX observations shown in Fig. 1, where uranium-bearing crystallites coat an iron-bearing particle. Micro-XANES analysis of metatorbernite gave a mean oxidation state of 5.7 ± 0.4 (Table 2, Supplementary Fig. 4). An additional uranyl-mica phase, parsonite $[Pb_2(UO_2)(PO_4)_2{\cdot}2H_2O]$; PDF 00-012-0259], was observed in particles of this sample, with a mean uranium oxidation state of 5.7 ± 0.4 (Table 2, Supplementary Fig. 4).

Uranium-bearing particles sampled from the Ochre Works location were identified as metavanuralite $(Al(UO_2)_2(VO_4)_2(OH){\cdot}8H_2O)$ (Supplementary Fig. 5d–f). This mineral was found to be closely associated with vanadian goethite [(Fe,V)OOH]; and muscovite–paragonite $(NaK_3(Al_{12}Si_{12}O_{40}(OH)_8)$. Metavanuralite, space group P1, is an uncommon uranyl mineral in the St. Austell region and, to our knowledge, has not previously been reported at South Terras. The archetypal location is the Mounana mine, Gabon, where it occurs as elongated crystals that form as crusts on goethite.[20,21] Due to the historical processing of iron ore at South Terras, the presence of goethite is not unexpected. Micro-XANES analysis of metavanuralite revealed a mean uranium oxidation state of 5.6 ± 0.4 (Table 2, Supplementary Fig. 4).

## DISCUSSION

The degradation of uraninite ore in vadose zone soils typically involves the formation of hydrated uranium oxides, uranyl-silicates, uranyl-carbonates and uranyl-phosphates.[22] Soluble uranyl ions can migrate from the primary ore body and other uranyl-bearing phases may be formed. At South Terras, ore

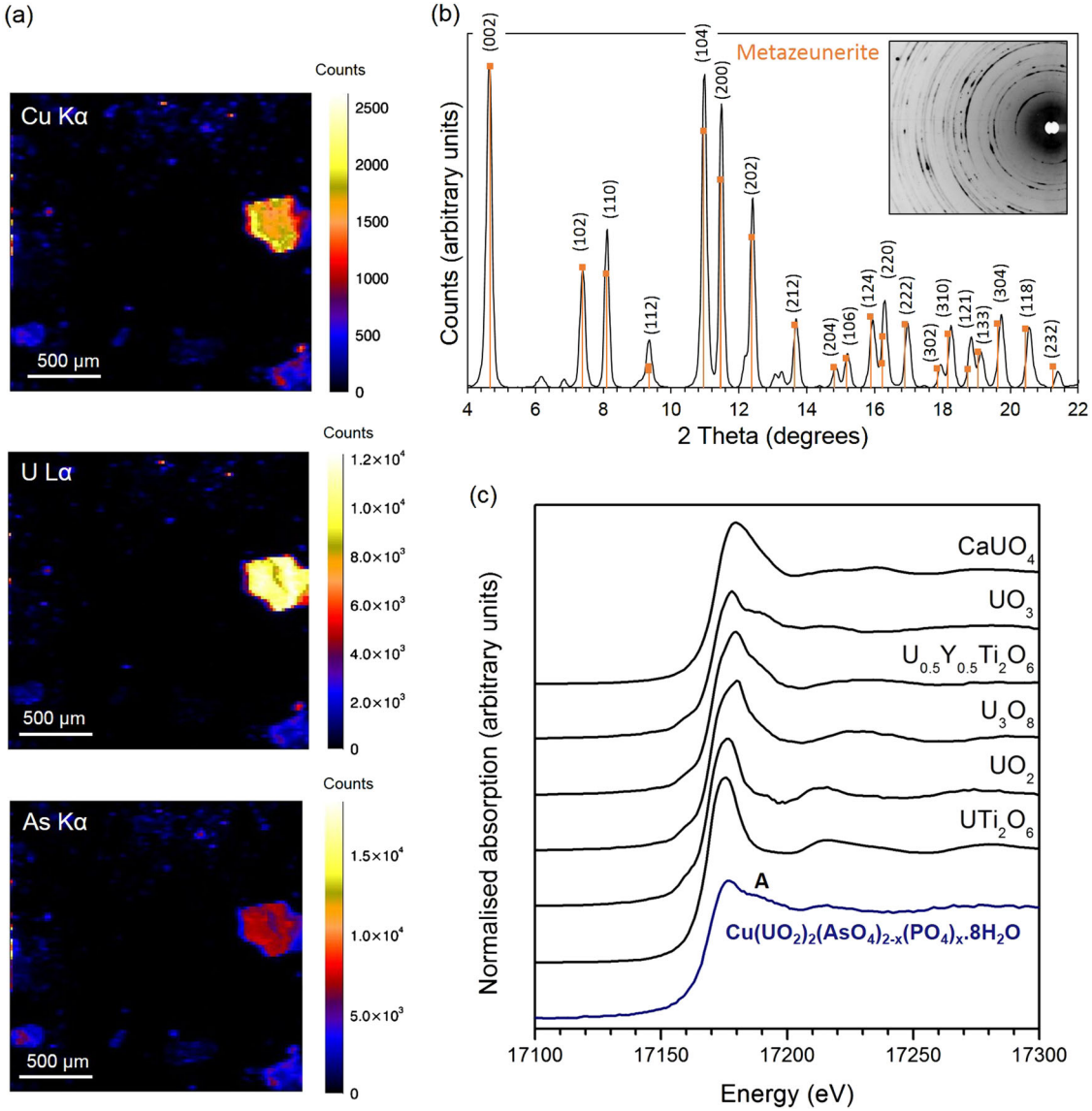


**Fig. 3** Analysis of particles from 25 cm at the Dressing Floor (DF) location using **a** μ-XRF mapping, revealed the association of uranium with copper and arsenic; **b** μ-XRD analysis confirmed a uranyl-mica structure similar to both metazeunerite ($Cu(UO_2)_2(AsO_4)_2{\cdot}8H_2O$) [PDF 00-004-0108] and metatorbernite ($Cu(UO_2)_2(PO_4)_2{\cdot}8H_2O$) [PDF 00-008-0309]; and **c** μ-XANES spectra taken at the U $L_{III}$ edge revealed an oxidation state predominantly of U(VI) when compared with known uranium-oxide standards. e.g.[30]

extraction processes and natural weathering of the country rock led to the proliferation of other elements during degradation, particularly arsenic and beryllium, which were found in significant concentrations (Table 1). The major uranium-bearing phases identified (across two sample locations and multiple sampling depths; 15 samples and at least three particles per sample) were the copper-bearing uranyl-arsenate and uranyl-phosphate phases, metazeunerite, metatorbernite, and their solid solution, in contrast to previous supposition.[4–6,23] The mechanism of uranium attenuation in these uranyl-micas is evident in Fig. 1; re-precipitation of mobile uranium, with arsenate and phosphate, as metazeunerite, metatorbernite, and their solid solution, is demonstrated by the presence of a copper, arsenic, phosphorus and uranium-bearing 'crust' coating the surfaces of silicon, aluminium, sulphur and iron-bearing minerals, for example, muscovite or jarosite.

Significantly, our data indicate that metazeunerite and metatorbernite were found to occur in solid solution, which has not been previously observed at other uranium-contaminated sites where uranyl-micas are present.[14–17] Owing to the higher solubility of uranyl-phosphate minerals compared with uranyl-arsenates (with solubility products of $10^{-12.8}$ and $10^{-49.2}$ for metatorbernite and metazeunerite, respectively),[24] it might be expected that arsenate end-members of this mineral family would dominate over the phosphate end-members, which is indeed observed in the Rietveld analysis of data shown in Fig. 3b, and composition inferred from interpolation of the unit cell volume of the end members. Remarkably, as a result of the complex environmental conditions brought about by the combined degradation of uranium ores and granitic lithologies at South Terras, arsenic contamination aids the attenuation of uranium through direct precipitation of metazeunerite—metatorbernite solid solution.

Metazeunerite and metatorbernite were found to be particularly concentrated at a depth of 25 cm (DF location), as highlighted by the high fractions of "recalcitrant and residual" copper, uranium, arsenic and phosphorus in the sequential extraction (Fig. 2, Supplementary Fig. 3). Indeed, concentrations of uranium were one order of magnitude greater at this depth (Table 1). This may be due to the presence of relatively undisturbed mine spoil at

**Table 2.** Mean oxidation state of uranium-bearing particles identified at South Terras, determined from the first derivative of the position of the uranium $L_{III}$-edge absorption spectrum, compared with the average oxidation state of U(IV–VI) compounds with similar chemical environments

| Location | Phase identified | Mean oxidation state |
|---|---|---|
| Ochre works, 0–2 cm | Metavanuralite ($Al(UO_2)_2(VO_4)_2(OH)\cdot 8H_2O$) | $5.6 \pm 0.4$ |
| Dressing floor, 25 cm | Meta(zeunerite/torbernite) solid solution ($Cu(UO_2)_2(AsO_4)_{2-x}(PO_4)_x\cdot 8H_2O$) | $5.9 \pm 0.4$ |
| Dressing floor, 25 cm | Metatorbernite ($Cu(UO_2)_2(PO_4)_2\cdot 8H_2O$) | $5.7 \pm 0.4$ |
| Dressing floor, 25 cm | Parsonite ($Pb_2(UO_2)(PO_4)_2\cdot 2H_2O$) | $5.7 \pm 0.4$ |
| Dressing floor, 0–2 cm | Non-crystalline uranium | $6.0 \pm 0.4$ |
| Dressing floor, 0–2 cm | Non-crystalline uranium | $5.0 \pm 0.4$ |

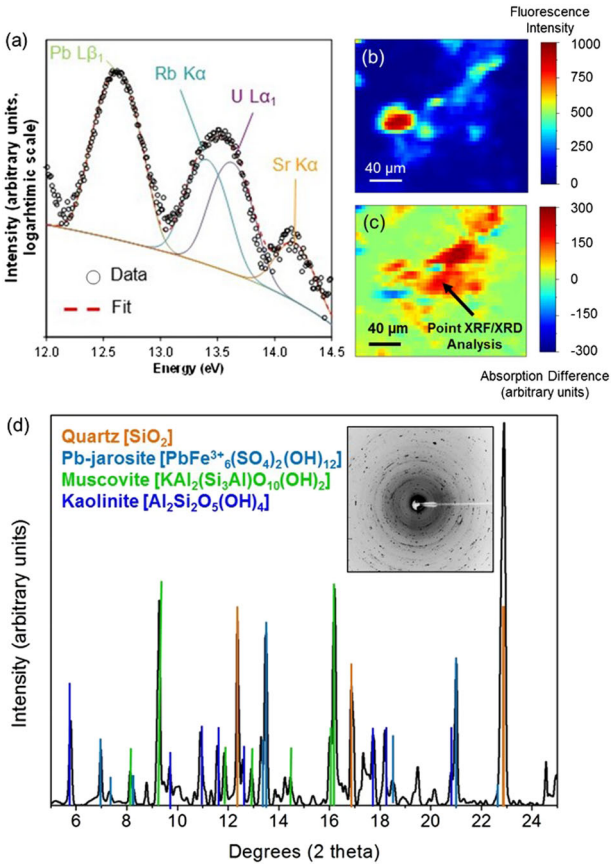


**Fig. 4** Micro-focus analysis of soil sample from the Dressing Floor location at 0–2 cm depth **a** illustrative Gaussian fits to the μ-XRF spectrum demonstrates the overlap between Rb Kα and U Lα1 fluorescence lines; **b** μ-XRF map of soil particles recording intensity above the U $L_{III}$ edge ($E_0 = 17.2$ keV); **c** ratio of the μ-XRF intensity at, and below ($E_0 = 16.9$ keV) the U $L_{III}$ edge; areas with intensity > 0 can be distinguished as containing uranium; and **d** μ-XRD analysis of uranium-rich point in (c), with patterns for quartz [PDF 04-016-2085], plumbojarosite [PDF 00-018-0698], muscovite [PDF 01-082-3731] and kaolinite [PDF 04-010-4800]

depth, or due to aqueous downward transport and precipitation of uranium, arsenic and phosphorous; either possibility confirms the potential for the entrapped micron-sized particles of metazeunerite/metatorbernite to control the long-term release of uranium at the site. At the surface, the speciation of uranium was markedly different; non-crystalline species with variable oxidation state dominated the DF location. The surface soils were enriched in phosphorus compared to at depth, by one order of magnitude (Table 1) and the sequential extraction showed that fractionally more uranium was associated with the reducible fraction at the surface than at depth (Fig. 2). This indicates that uranyl-phosphates, likely bound to iron-bearing phases, may be present at the surface, however the presence of uranyl-carbonates or uranyl species bound to organics cannot be ruled out. Nevertheless, it seems likely that the surface fraction of uranium shows a higher mobility than that associated with metazeunerite and metorbernite, sequestered at depth.

Interestingly, there was a clear difference in the uranium concentration and mineralogy at the Ochre Works and Dressing Floor areas of comparable depths; uranyl mica phases were ubiquitous in the samples taken from the Dressing Floor (at all depths sampled), while the soils from the Ochre works area exhibited much lower uranium content, which was associated with oxidised iron and vanadium (Table 2, Supplementary Fig. 4). These differences are clearly associated with the different degradation mechanisms of uranium arising from different ore processing methods; chemical extraction at the Dressing Floor location, and smelting at the Ochre Works location. With the predominant groundwater flow direction from the Dressing Floor towards the Ochre Works and the River Fal,[4,23] the absence of significant uranium content in the Ochre Works indicates the potential efficacy of the uranyl-micas for attenuation of uranium at the site.

Sequestration of uranium in complex mineralogical assemblages at South Terras is the result of a set of rather unique geological conditions. To identify this remediation mechanism at other sites, where arsenic and uranium are key co-contaminants, further detailed mineralogical assessments are required. These should be considered as an essential input to understand the ultimate environmental fate of degraded uranium ore.

## METHODS

### Site and soil sampling

South Terras is located in the St. Austell District of Cornwall (SW England, Supplementary Fig. 1a) where uranium mining operations were performed near Tolgarrick Mill (Supplementary Fig. 1b). The location is a Site of Special Scientific Interest (SSSI) with restricted access. Detailed site information regarding the geology, stratigraphy and spatial variations in soil, groundwater and stream water chemistry (e.g., cation concentrations and pH) are given by Read et al.,[4] Sideeg et al.,[5] and Hooker et al.[23] Two well-documented sites, the Ochre Works (OW) and Dressing Floor (DF) locations, were selected for investigation (Supplementary Fig. 1b) to understand how ore processing influenced the degradation of uranium ore and subsequent uranium speciation in the soil. The former is where iron-ore was once smelted and the latter is where uranium-ore and mine spoil processing occurred.[1] Spoil processing involved sequential chemical treatments using HCl, $H_2SO_4$, $BaSO_4$, $NaHCO_3$, $NH_4$, NaOH and hydrobromic acid[1]. The site is heavily vegetated, with a surface dark-brown mineral/organic soil horizon (0–15 cm, Supplementary Fig. 1c), beneath which lays mine spoil interspersed with a hematitic sand (to ~50 cm)[6]. These sequences are underlain by kaolinitic clay.[24] A series of samples, taken from locations 10–20 m apart, were collected, by hand, at the surface (0–2 cm depth) from both sample locations, and at a shallow depth (25 cm) at the DF location.

### Soil preparation and bulk characterisation

Soils were dried in air and sieved to a particle size of <300 µm, removing organic litter. Thinly spread soils were screened to localise radioactive particles for further analysis using autoradiography (Packard Instant Imager). Portions of soil containing radioactive 'hotspots' were collected onto adhesive carbon tabs for SEM analysis or kapton tape for synchrotron analyses. Back scattered electron imaging was performed using a Hitachi TM3030 with an accelerating voltage of 15 kV with coupled EDX analysis using a Quantax 70 EDX detector. Samples were analysed in variable pressure mode (no coating required). Bulk XRD analysis was performed using a Bruker D2 Phaser diffractometer, operating in reflection mode at 40 kV and 30 mA with Cu Kα radiation. Data were acquired between $5 < 2\theta < 60°$ at 2° $min^{-1}$ and a step size of 0.02°.

### µ-XRF, µ-XRD and µ-XANES analysis

Synchrotron radiation micro-focus analyses were conducted at the now decommissioned X27A beamline at the National Synchrotron Light Source (NSLS, USA) and at the microXAS (X05LA) beamline at the Swiss Light Source (SLS). At NSLS, the soil particles, mounted between two films of kapton tape, were oriented at 45° to the direction of x-ray propagation and raster scanned through the micro-focused x-ray beam (spot size of ~7 × 14 µm). X-ray fluorescence (XRF) was measured using a four-element silicon drift detector (Hitachi) mounted at 90° to the incident x-ray beam direction. Uranium $L_{III}$-edge ($E_0 = 17.166$ keV) µ-XANES (X-ray Absorption Near-Edge Structure) spectra were recorded in fluorescence mode by monitoring the U $L\alpha_1$ emission (13.614 keV). Two-dimesional micro-x-ray diffraction (µ-XRD) measurements were acquired using a CCD camera (Bruker SMART 1500) positioned 235 mm behind the sample and calibrated to an alumina $Al_2O_3$ standard (NIST SRM676a)[25]. At a monochromatic beam energy of 17.200 keV, the wavelength was 0.7093 Å.

At SLS, µ-XAS data were collected according to the methodology detailed by Crean et al.[25,26] The monochromatic beam energy was identical to NSLS. Fluorescence µ-XANES spectra of uranium standards ($UTi_2O_6$, $UO_2$, $U_{0.5}Y_{0.5}Ti_2O_6$, $U_3O_8$, $UO_3$ and $CaUO_4$) were measured to aid interpretation.

### Sequential extraction

A modified version of the Community Bureau of Reference (BCR) scheme,[27] previously applied to uranium speciation in soils,[28,29] was used. The distribution of uranium was defined in five phases: exchangeable, reducible, oxidisible and recalcitrant and residual. A separate aliquot was digested in aqua regia/HF to determine the concentration of each element in the soil. The residual fraction represents the elemental concentration of the total digest, less the elemental concentration of the other extraction steps combined. The extraction and digest reagents and procedure are summarised in Supplementary Table 2. Ten replicate experiments using 0.5 g soil were analysed, in addition to duplicate blanks. After each extraction step, samples were centrifuged (3000 r.p.m., 15 min), the supernatant removed and acidified with concentrated $HNO_3$. All extract solutions were analysed for major and minor elements by ICP-AES (Spectro Ciros Vision).

### Data availability

The data that support the findings of this study are available from the corresponding author upon reasonable request.

## ACKNOWLEDGEMENTS

The authors wish to acknowledge Natural England and the St. Stephen Estate for granting access to the South Terras SSSI. We wish to thank Mr. Neil Bramall and Mrs. Irene Johnson for technical support. We acknowledge support from the UK Government Department of Energy and Climate Change, through the award of the MIDAS Collaboratory, for analytical equipment. Portions of this work were performed at Beamline X27A, NSLS, Brookhaven National Laboratory. X27A is supported in part by the U.S. Department of Energy (DOE)—Geosciences (DE-FG02-92ER14244 to The University of Chicago—CARS). Use of the NSLS was supported by the DOE, Office of Science, under Contract No. DE-AC02-98CH10886. Access to the Swiss Light Source, Paul Scherrer Institute, Villigen, Switzerland, was supported by the TALISMAN collaborative project, with co-funding from the European Commission under the Euratom Research and Training Programme on Nuclear Energy, within the 7th Framework programme (grant agreement 323300). We wish to acknowledge EPSRC for the award of an ECR Fellowship (EP/N017374/1), and for funding on the Nuclear FiRST CDT (EP/G037140/1). Thanks are given to Dr. Eric Pierce for his help in improving the manuscript through the review process.

## AUTHOR CONTRIBUTIONS

All authors provided substantial contributions to conception of the research performed, or the acquisition, analysis or interpretation of the data; they drafted or revised the manuscript; approved the final version and; are accountable for the accuracy and integrity of the data and its interpretation.

## ADDITIONAL INFORMATION

**Supplementary information** accompanies the paper on the *npj Materials Degradation* website (https://doi.org/10.1038/s41529-017-0019-9).

**Competing interests:** The authors declare no competing financial interests.

**Publisher's note:** Springer Nature remains neutral with regard to jurisdictional claims in published maps and institutional affiliations.

## REFERENCES

1. Smale, C. V. Cornwall's premier uranium and radium mine. *J. Royal Inst. Cornwall* **184**, 304–322 (1992).
2. Collins, J. H. Observations on the West of England Mining Region. *Trans. Royal Geol. Soc. Cornwall* (1912).
3. Dines, H. G. The metalliferous mining region of South West England. *Mem. Geol. Surv. Great Brit.* **2**, 541–543 (1956).
4. Read, D., Hooker, P. J., Ivanovich, M. & Milodowski, A. E. A natural analogue study of an abandoned uranium mine in Cornwall, England. *Radiochim. Acta* **52/53**, 349–356 (1991).
5. Sideeg, S. M., Bryan, N. D. & Livens, F. R. Behaviour and mobility of U and Ra in sediments near an abandoned uranium mine, Cornwall, UK. *Environ. Sci. Proc. Impact.* **17**, 235–245 (2015).
6. Moliner-Martinez, Y., Campins-Falco, P., Worsfold, P. J. & Keith-Roach, M. The impact of a disused mine on uranium transport in the River Fal, South West England. *J. Environ. Monitoring* **6**, 907–913 (2004).
7. Pablo, J. D. et al. The oxidative dissolution mechanism of uranium dioxide. I. The effect of temperature in hydrogen carbonate medium. *Geochim. Cosmochim. Acta* **63**, 3097–3103 (1999).
8. Beamish, D., Howard, A. S., Ward, E. K., White, J. & Young M. E. Tellus South West airborne geophysical data. Natural Environment Research Council, British Geological Survey Report OR/14/014 (2014).
9. Middleton, D. R. S. et al. Urinary arsenic profiles reveal exposures to inorganic arsenic from private drinking water supplies in Cornwall, UK. *Sci. Rep.* **6**, 25656 (2016).
10. Hanic, F. The crystal structure of meta-zeunerite $Cu(UO_2)_2(AsO_4)_2.8H_2O$. *Czech J. Phys. B.* **10**, 169–181 (1960).
11. Locock, A. J. & Burns, P. C. Crystal structures and synthesis of the copper-dominant members of the autunite and meta-autunite groups: torbernite, zeunerite, metatorbernite and metazeunerite. *Can. Min.* **41**, 489–502 (2003).
12. Da Silva, J. R. R. & Williams, R. J. P. (eds) *The Biological Chemistry of the Elements: The Inorganic Chemistry of Life* (Oxford University Press, 1997).
13. Locock, A. J. & Burns, P. C. Monovalent cations in structures of the meta-autunite group. *Can. Min.* **42**, 973–996 (2004).
14. Catalano, J. G. et al. Changes in uranium speciation through a depth sequence of contaminated handford sediments. *Environ. Sci. Technol.* **40**, 2517–2524 (2006).
15. Arai, Y., Marcus, M. A., Tamura, N., Davis, J. A. & Zachara, J. M. Spectroscopic evidence of uranium bearing precipitates in vadose zone sediments at the Hanford 300-Area site. *Environ. Sci. Technol.* **41**, 4633–4639 (2007).
16. Singer, D. M., Zachara, J. M. & Brown, G. E. Jr. Uranium speciation as a function of depth in contaminated Hanford sediments–A micro-XRF, micro-XRD and micro- and bulk-XAFS study. *Environ. Sci. Technol.* **43**, 630–636 (2009).
17. Stubbs, J. E. et al. Newly recognised hosts for uranium in the Hanford site vadose zone. *Geochim. Cosmochim. Acta* **73**, 1563–1576 (2009).
18. Purvis, O. W., Bailey, E. H., McLean, J., Kasama, T. & Williamson, B. J. *Geomicrobiol. J.* **21**, 159–167 (2004).
19. Stone, M. The tregonning granite: petrogenesis of Li-mica granites in the Cornubian batholith. *Miner. Mag.* **56**, 141–155 (1992). 383.
20. Cesbron, F. Nouvelles donnees sur la vanuralite. Existence de la metavanuralite. *Bull. Soc. Fr. Minér. Cristallogr.* **93**, 242–248 (1970).
21. Lauf, R. J. *Mineralogy of uranium and thorium* (Schiffer Publishing, 2016).
22. Frondel, C. Study of uranium minerals: gummite. *Bull. Geol. Soc. Am.* **63**, 1252–1253 (1952).

23. Hooker, P. J. et al. *A radionuclide migration study at the disused South Terras uranium mine*, Cornwall. DOE Report WE/89/13 (1989).
24. Vochten, R. & Goeminne, A. Synthesis, crystallographic data, solubility and electrokinetic properties of meta-zeunerite, meta-kirchheimerite and nickel-uranylarsenate. *Phys. Chem. Miner.* **11**, 95–100 (1984).
25. Crean, D. E. et al. Microanalytical X-ray imaging of depleted uranium speciation in environmentally aged munitions residues. *Environ. Sci. Technol.* **48**, 1467–1474 (2014).
26. Crean, D. E. et al. Expanding the nuclear forensic toolkit: chemical profiling of uranium ore concentrate particles by synchrotron X-ray microanalysis. *RSC Adv.* **5**, 87908–87918 (2015).
27. Ure, A. M., Quevauviller, P., Muntau, H. & Griepink, B. Speciation of heavy metals in soils and sediments. An account of the improvement and harmonisation of extraction techniques undertaken under the auspices of the BCR of the commission of the european communities. *Int. J. Environ. Anal. Chem.* **51**, 135–151 (1993).
28. Oliver, I. W., Graham, M. C., MacKenzie, A. B., Ellam, R. M. & Farmer, J. G. Distribution and partitioning of depleted uranium (DU) in soils at weapons test ranges–investigations combining the BCR extraction scheme and isotopic analysis. *Chemosphere* **72**, 932–939 (2008).
29. Crean, D. E. et al. Remediation of soils contaminated with particulate depleted uranium by multi-stage chemical extraction. *J. Haz. Mater.* **263**, 382–390 (2013).
30. Pierce, E. M., Icenhower, J. P., Serne, R. J. & Catalano, J. G. Experimental determination of $UO_{2(cr)}$ dissolution kinetics: Effects of solution saturation state and pH. *J. Nucl. Mater.* **345**, 206–218 (2005).